

Article

Effect of V and Ti on the Oxidation Resistance of WMoTaNb Refractory High-Entropy Alloy at High Temperatures

Shuaidan Lu , Xiaoxiao Li, Xiaoyu Liang, Wei Yang and Jian Chen *

School of Materials Science and Chemical Engineering, Xi'an Technological University, Xi'an 710021, China; lushuaidan@hotmail.com (S.L.); lixiaoxiao_stu@163.com (X.L.); liangxiaoyu@st.xatu.edu.cn (X.L.); yangwei_smx@163.com (W.Y.)

* Correspondence: chenjian@xatu.edu.cn

Abstract: Alloying with V and Ti elements effectively improves the strength of WMoTaNb refractory high entropy alloys (RHEAs) at elevated temperatures. However, their effects on the oxidation resistance of WMoTaNb RHEAs are unknown, which is vitally important to their application at high temperatures. In this work, the effect of V and Ti on the oxidation behavior of WMoTaNb RHEA at 1000 °C was investigated using a thermogravimetric system, X-ray diffraction and scanning electron microscopy. The oxidation of all alloys was found to obey a power law passivating oxidation at the early stage. The addition of V aggravates the volatility of V_2O_5 , MoO_3 and WO_3 , and leads to disastrous internal oxidation. The addition of Ti reduces the mass gain in forming the full coverage of passivating scale and prolongs the passivation duration of alloys.

Keywords: metals and alloys; oxidation; corrosion; surfaces



Citation: Lu, S.; Li, X.; Liang, X.; Yang, W.; Chen, J. Effect of V and Ti on the Oxidation Resistance of WMoTaNb Refractory High-Entropy Alloy at High Temperatures. *Metals* **2022**, *12*, 41. <https://doi.org/10.3390/met12010041>

Academic Editor: Oleg N. Senkov

Received: 7 December 2021

Accepted: 23 December 2021

Published: 25 December 2021

Publisher's Note: MDPI stays neutral with regard to jurisdictional claims in published maps and institutional affiliations.



Copyright: © 2021 by the authors. Licensee MDPI, Basel, Switzerland. This article is an open access article distributed under the terms and conditions of the Creative Commons Attribution (CC BY) license (<https://creativecommons.org/licenses/by/4.0/>).

1. Introduction

Refractory high entropy alloys (RHEAs) were reported to possess excellent mechanical properties at elevated temperatures and high thermal stability, making them extremely promising high-temperature structural materials [1–3]. In reported RHEAs, WMoTaNb is famous for retaining high strength above 400 MPa at temperatures up to 1600 °C and has a great potential for high temperature applications; however, its compressive plastic strain at room temperature (RT) is inferior at 3%, severely limiting its processing formation performance [4]. The microstructure and performance of RHEAs can be changed dramatically by alloying other elements [5–7]. It is reported that alloying with V effectively improves the strength of WMoTaNb alloys to approximately 200 MPa at elevated temperatures of 600 °C–1200 °C [4]. Alloying with Ti is found to improve both the strength (46% higher than WMoTaNb) and ductility (11.5% and five times higher than that of WMoTaNb) of WMoTaNbTi alloy at room temperature by solid solution hardening effect and grain-boundary cohesion improvement [8].

The investigation of WMoTaNb alloys has been focused on their structure and mechanical properties; however, the oxidation behaviors of these alloys at elevated temperatures determine the application and have rarely been studied [9,10]. It is known that RHEAs, especially WMoTaNb alloys, suffer from poor oxidation resistance at elevated temperatures, which may be attributable to the evaporation of volatile oxides (MoO_3 , WO_3 and V_2O_5) and the scale fractures caused by the high Pilling–Bedworth ratio (PBR) of Ta_2O_5 (2.47) and Nb_2O_5 (2.74) [11–14]. Researchers have undertaken a large number of studies on improving the oxidation resistance of HEAs by alloying beneficial elements, such as Al, Ti, Cr and Si [15–18]. Gorr and Lo found that a $CrTaO_4$ -based oxide layer can provide long-term oxidation resistance for RHEAs at elevated temperatures [19,20]. In this work, an attempt has been made to investigate the effect of V and Ti on the oxidation behavior of WMoTaNb RHEAs at elevated temperatures and to explain the associated oxidation mechanism.

2. Materials and Methods

WMoTaNb, WMoTaNbV and WMoTaNbTi RHEAs were prepared by vacuum induction levitation melting from high purity (>99.9 wt.%). Each prepared ingot was remelted six times to ensure alloy homogenization. The chemical composition of these alloys is measured by EPMA and summarized in Table 1. The discrepancy between the experimental composition of RHEAs as cast here and their normal composition is due to the different saturated vapor pressure of elements. In the studied RHEAs, W has a lower saturated vapor pressure than Ti or V, leading to the lower volatilization of W compared to other elements. This phenomenon has also been reported in the study of WMoTaNb RHEA by Senkov [4]. The resulting ingots were cut into small samples (4.5 mm × 4.5 mm × 2 mm) by electrical discharge machining. Subsequently, these samples were polished to 2000# and ultrasonically cleaned in ethanol. In order to limit the undesirable edge effect, the size of samples was controlled to be as uniform as possible. The structures of the three alloys was investigated by X-ray diffraction (XRD, Bruker D8, Bruker AXS, Karlsruhe, Germany, Cu-K α radiation) and scanning electron microscopy (SEM, QuantaFEG400, FEI, Hillsboro, OR, USA). The prepared samples were put in a thermogravimetric system (TG-DSC, STA449F3, Netzsch, Germany) to conduct isothermal oxidation tests. The oxidation condition was set to 1000 °C in dry air (>99.999 vol.% pure, 50 mL·min⁻¹) and the heating rate was fixed at 10 °C/min to ensure uniform isothermal oxidation and make the comparative study reliable. The blank sample test was conducted before the isothermal oxidation experiments, and deducted in the final mass change curves. Each isothermal oxidation test was carried out until complete oxidation.

Table 1. Chemical composition of the three alloys measured by EPMA (in at.%).

RHEA	W	Mo	Ta	Nb	V	Ti
WMoTaNb	28.2	23.3	26.5	22.1	-	-
WMoTaNbV	22.7	19.5	22.2	17.8	17.8	-
WMoTaNbTi	26.4	18.0	23.4	17.1	-	15.1

According to the reported studies, the oxidation behavior of alloys can be described by a power law equation as follows:

$$\left(\frac{\Delta m}{A}\right) = Kt^n \quad (1)$$

where Δm is the oxidation mass change and A and t are the total surface area of the sample and exposure duration, respectively. K is the oxidation coefficient and n is the oxidation exponent. It is generally acknowledged that passivating oxidation behavior consists of the formation and growth of the passivating scale. Researchers suggest that the oxidation coefficient (K) and the oxidation exponent (n) stand for the mass gain of forming the full coverage of passivating scale and the growth rate of the passivating scale, respectively [21]. According to Equation (1), when $n = 1$, the power law equates linear law behavior; when $n = 0.5$, it complies with parabolic law oxidation; when $n = 1/3$, it conforms to the cubic law [22].

3. Results and Discussion

It can be seen in Figure 1a–c that all of the as-cast alloys present dendrite (DR) and interdendrite (ID) structures. The average grain size in as-cast WMoTaNb, WMoTaNbV and WMoTaNbTi RHEAs is 50 μm , 30 μm and 18 μm , respectively. The difference in cooling rates during solidification not being significant indicates the grain refinement of V and Ti on the WMoTaNb RHEA. The XRD patterns indicate that the three alloys all had a single-phase BCC structure. With the addition of V, the BCC peaks are broadened and shift to higher 2θ , and the lattice constant decreases from 0.3215 nm to 0.3179 nm. The XRD peak broadening was likely due to the lattice strain caused by lattice distortion, which is

frequently found in the solid solution structure of HEAs. The decreased lattice constant is due to the solute V, with the smallest radius (1.35 Å) compared with the other elements in WMoTaNbV RHEAs. The addition of Ti has little impact on the lattice constant due to its similar radius to the other elements (seen in Table 2).

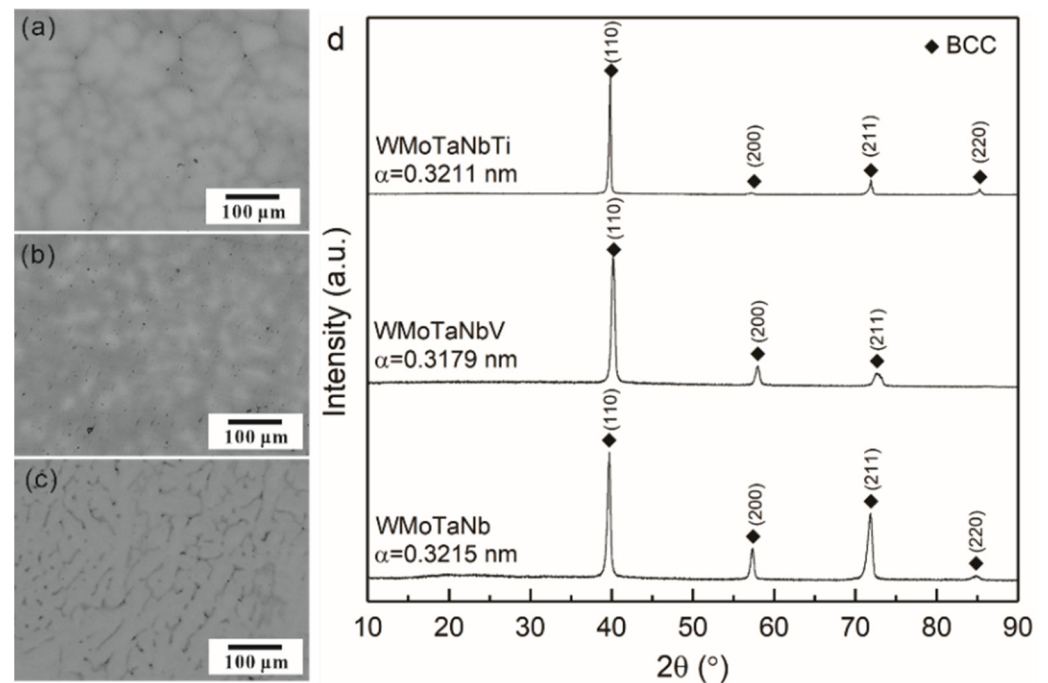


Figure 1. BSE micrographs and XRD patterns (d) of as-cast (a) WMoTaNb, (b) WMoTaNbV and (c) WMoTaNbTi alloys.

Table 2. The radius of elements of the three alloys.

Element	W	Mo	Ta	Nb	V	Ti
Radius (Å)	1.41	1.40	1.48	1.48	1.35	1.45

A power-law equation was applied to describe each kinetics curve, and the fitted curves in Figure 2 are marked with red and dotted lines. It can be clearly seen in Figure 2 that the mass gain continues to decrease after the prolonged oxidation. The descending mass change is due to the ending of oxidation and the volatilization of some oxides. This state is suggested to be completely oxidized, and has been reported by Müller et al. [23]. The initial power law kinetics indicate the oxides formed in the early stage can provide effective protection from further oxidation. It can be seen clearly in Figure 2 that the mass gain of alloys at the initial linear stage decreases with the addition of Ti and increases with the addition of V, which indicates that the mass gain in forming a passivating oxide layer is reduced by the addition of Ti and increased by the addition of V. Besides this, the oxidation exponent (n) of the power law is found to increase with the addition of V and Ti, indicating a higher growth rate of the oxide layer. The oxidation exponent (n) of a V-containing alloy is higher than that of a Ti-containing alloy, showing worse oxidation resistance. In addition, the ranges of fitted power laws represent the passivation duration, and those of WMoTaNb, WMoTaNbV and WMoTaNbTi RHEAs are 8 h, 10 h and 5 h, respectively. The shorter passivation duration of WMoTaNbV could be attributed to the severe volatility of V_2O_5 , which allowed oxygen in-diffusion and resulted in complete oxidation. The passivation duration of WMoTaNb was prolonged by the addition of Ti from 8 h to 10 h, which benefits from the improvement in scale adhesion. However, the higher oxidation rate of the passivating oxide layer indicates that the internal oxidation of

the alloy was aggravated by the addition of Ti. The total mass gain of WMoTaNbTi RHEA after complete oxidation was higher than that of other RHEAs, which was likely due to less W and Mo forming volatile oxides. The lower mass gain of WMoTaNbV compared to other samples should be attributed to the evaporation of volatile V, Mo and W oxides.

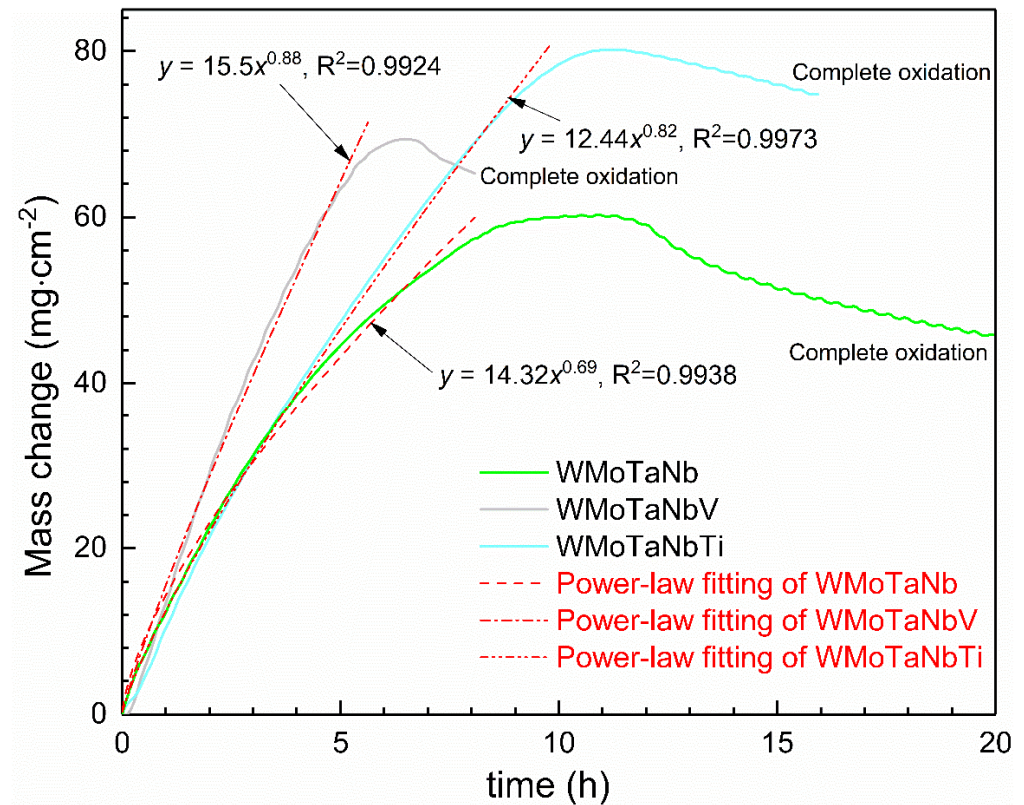


Figure 2. The oxidation kinetics of WMoTaNb, WMoTaNbV and WMoTaNbTi RHEAs during isothermal exposure to dry air at 1000 °C.

Figure 3 is the XRD patterns of oxide scales formed on the three alloys after 0.5 h and 4 h oxidation. The WMoTaNbV sample oxidized for 4 h was hideously deformed and unfit for an XRD test. As the WMoTaNbV was oxidized sufficiently after the initial 0.5 h, the surface XRD after further oxidation did not make sense and is not shown in Figure 2. As shown in Figure 3, after an initial 0.5 h of oxidation at 1000 °C, Nb₂O₅, Ta₂O₅ and WO₃ phases were found on the surface of the WMoTaNb RHEA. With a progressive oxidation duration of 4 h, the oxides on the surface mainly consisted of Nb₂O₅ and some Ta₂O₅. The WO₃ phase was observed after the initial 0.5 h, which is due to the low volatilization rate of WO₃ at 1000 °C. The surface being replete with Nb₂O₅ after further oxidation should be attributed to the fast kinetic rate of Nb out-diffusion. The oxides formed on the surface of WMoTaNbV RHEA after the first 0.5 h vary from those of WMoTaNb, and mainly consist of Ta₁₈V₄O₅₅. β-Ta₂O₅ was found to transform into nine Ta₂O₅·2V₂O₅ (Ta₁₈V₄O₅₅) with V₂O₅ at elevated temperatures, which can explain the mass gain of WMoTaNbV being higher than that of WMoTaNb after complete oxidation [24]. The addition of Ti leads to the complex scale of Nb₂O₅, TiO₂ and Ta₂O₅ in the further oxidation. Based on the theory of the Pilling–Bedworth ratio for metals, the PBR values of oxides formed in this study were calculated and summarized in Table 3 [25,26]. It is obvious that the PBR value of TiO₂ was significantly less than that of the other oxides, which can effectively relieve the interstress of the scales.

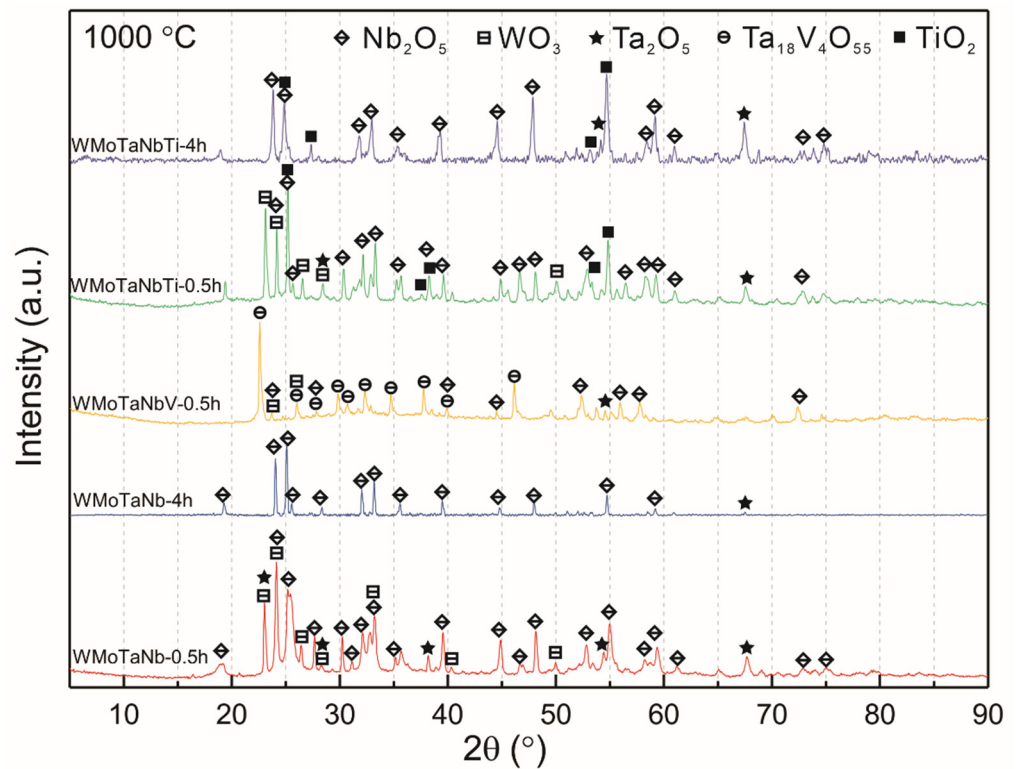


Figure 3. XRD patterns of the oxide scales formed on three alloys after different oxidation times at 1000 °C.

Table 3. Data used to calculate PBR and the PBR values of corresponding oxides.

Material	Crystal System	W (g) Mole Weight	ρ (g·cm ⁻³)	ICSD	PBR
W	Cubic	183.9	19.25	653430	-
Mo	Cubic	95.94	10.2	162278	-
Ta	Monoclinic	180.9	16.29	96594	-
Nb	Cubic	92.91	8.37	170906	-
V	Cubic	50.94	6.11	260470	-
Ti	Hexagonal	47.88	4.65	99778	-
WO ₃	Tetragonal	231.9	6.65	89092	3.65
MoO ₃	Orthorhombic	143.94	4.71	166362	3.25
Ta ₂ O ₅	Tetragonal	441.8	8.17	157683	2.43
Nb ₂ O ₅	Monoclinic	265.82	4.55	16605	2.63
V ₂ O ₅	Monoclinic	181.88	4.16	156054	2.62
TiO ₂	Tetragonal	79.88	4.26	165925	1.82

As seen in Figure 4, the scales formed on the surface of WMoTaNb were homogeneous and flat, except for many pores and a few cracks. By combining the results of XRD and EDS (seen in Table 4), the oxide particles can be inferred to be Nb₂O₅, Ta₂O₅ and WO₃. The pores present on the scales can be attributed to the volatilization of MoO₃ and WO₃. The surface of WMoTaNbV RHEA varied from that of WMoTaNb and was full of tiny tubules and some larger ones. The surface of WMoTaNbTi RHEA was also different from that of WMoTaNb and had many more cracks. The white mounds near the cracks can be inferred to be Ta₂O₅ from the EDS results. According to the elemental distribution mapping, the oxide scales of WMoTaNb, WMoTaNbV and WMoTaNbTi RHEAs were enriched with oxygen, and were measured from the O profiles to be about 15.4 μ m, 346 μ m and 43 μ m in thickness, respectively. It is clear that the thickness of the oxide scale increased with the addition of V and the addition of Ti, indicating worse oxidation resistance. It is worth noting that the oxide scale of the V-containing alloy was porous and had a rugged surface,

which may have been caused by the severe volatility of V_2O_5 , MoO_3 and WO_3 , and resulted in disastrous internal oxidation. The increased cross-sectional thickness of WMoTaNbTi RHEA can be ascribed to the large cracks observed on the surfaces (Figure 4c), which led to massive oxygen ingress and resulted in severe internal oxidation. The relatively dense scale of WMoTaNbTi reduced the volatile oxidation, which led to the volume expansion of the internal scale and resulted in the cracks of the outer scales

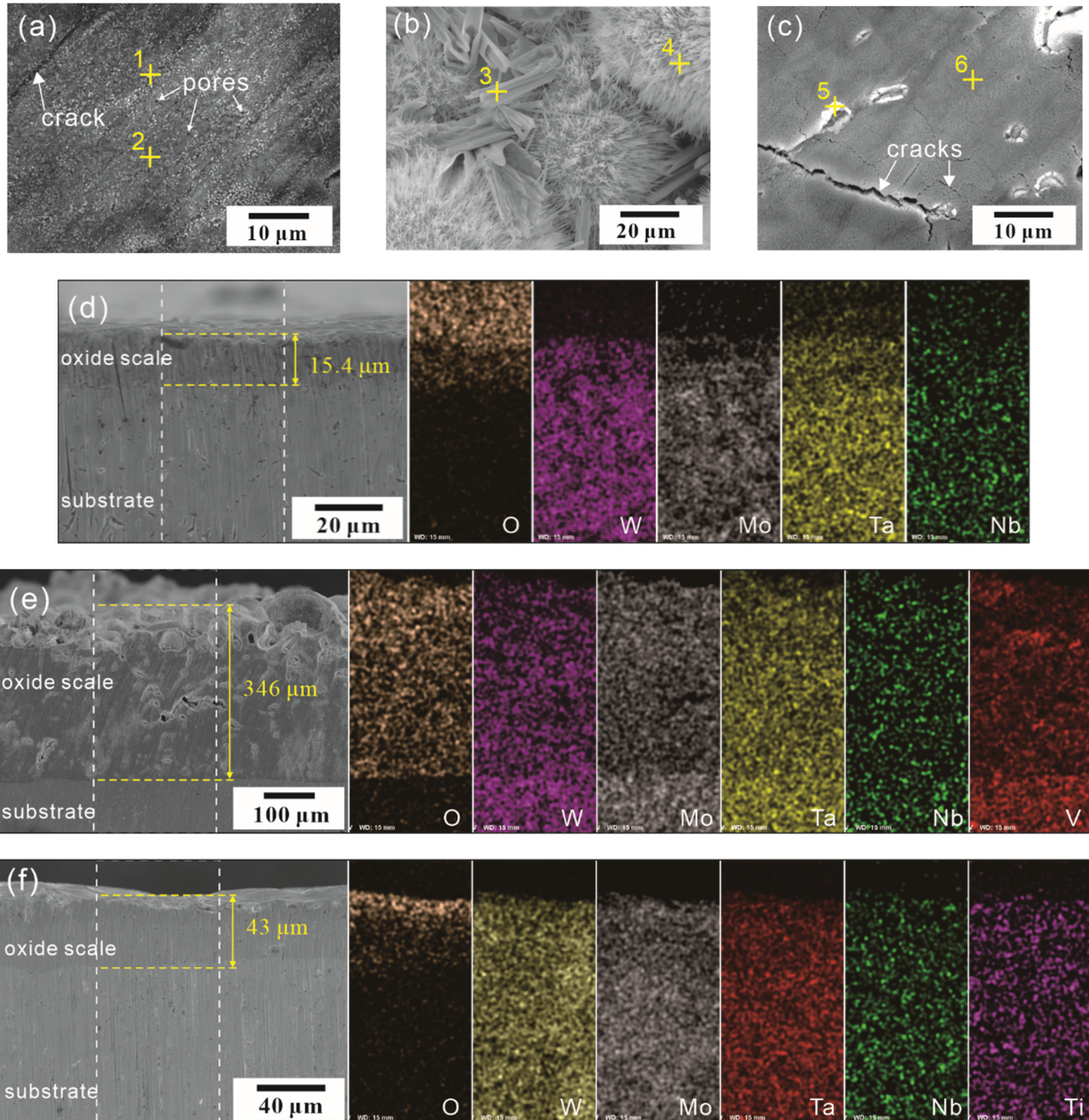


Figure 4. Surface morphologies, cross sections and EDS results of (a,d) WMoTaNb, (b,e) WMoTaNbV and (c,f) WMoTaNbTi RHEAs after 0.5 h of oxidation at 1000 °C.

Table 4. Quantitative results for the EDS point analysis of the spots noted in Figure 4 (at %).

Spot	O	W	Mo	Ta	Nb	V	Ti
1	89.8	-	-	4.3	5.9	-	-
2	70.5	9.2	-	10.4	9.9	-	-
3	86.5	-	-	11.0	-	2.6	-
4	55.0	8.9	1.5	13.7	17.5	3.3	-
5	86.9	-	-	13.1	-	-	-
6	77.7	8.5	-	7.2	6.6	-	-

4. Conclusions

The effects of V and Ti on the oxidation behavior of WMoTaNb RHEA at 1000 °C were investigated. The oxidation of WMoTaNb, WMoTaNbV and WMoTaNbTi RHEAs all obeyed a power law oxidation kinetic at the early stage. The SEM/EDS results and oxidation kinetic indicate that WMoTaNb RHEA had the best oxidation resistance. The addition of V was found to aggravate the volatility of V₂O₅, MoO₃ and WO₃, and result in disastrous internal oxidation. The addition of Ti reduced the mass gain in forming the full coverage of passivating scale and prolonged the passivation duration of the alloys, which is attributed to the decreased PBR of oxides and the relief of interstress.

The results obtain in this paper indicate that the oxidation resistance of WMoTaNb, WMoTaNbTi and WMoTaNbV is poor at high temperature. In our following works, the effect of the addition of Si and Y, aiming at the improvement of the oxidation resistance of WMoTaNb RHEA, will be studied. In addition, micro-arc oxidation (MAO) and plasma spraying coatings on the surface of WMoTaNb RHEA to improve the oxidation resistance will be investigated in our future works.

Author Contributions: Conceptualization, S.L. and J.C.; methodology, X.L. (Xiaoyu Liang); validation, X.L. (Xiaoyu Liang); formal analysis, X.L. (Xiaoxiao Li); investigation, X.L. (Xiaoxiao Li); writing—original draft preparation, S.L.; writing—review and editing, W.Y.; supervision, J.C.; project administration, J.C. All authors have read and agreed to the published version of the manuscript.

Funding: This work was financially supported by the National Natural Science Foundation of China (Grant No. 51931005, 52071251), Shaanxi Outstanding Youth Fund (2020JC-49) and Youth Innovation Team of University in Shaanxi Province, Natural Science Basic Research Program of Shaanxi (Program No. 2021JQ-645) and Scientific Research Program Funded by Shaanxi Provincial Education Department (Program No. 20JK0684).

Institutional Review Board Statement: Not applicable.

Informed Consent Statement: Not applicable.

Data Availability Statement: The data used to support the findings of this study are available from the corresponding author upon request.

Conflicts of Interest: The authors declare no conflict of interest.

References

- Lee, C.; Kim, G.; Chou, Y.; Musicó, B.L.; Gao, M.C.; An, K.; Song, G.; Chou, Y.-C.; Keppens, V.; Chen, W.; et al. Temperature dependence of elastic and plastic deformation behavior of a refractory high-entropy alloy. *Sci. Adv.* **2020**, *6*, eaaz4748. [[CrossRef](#)]
- Senkov, O.N.; Miracle, D.B.; Chaput, K.J.; Jean-Philippe, C.J. Development and exploration of refractory high entropy alloys-A review. *J. Mater. Res.* **2018**, *33*, 3092–3128. [[CrossRef](#)]
- Ostovari Moghaddam, A.; Zharebtsov, D.; Shaburova, N.A.; Trofimov, E.A. Single-Phase Medium- to High-Entropy Alloys Developed by a Simple Thermodynamic Approach. *JOM* **2021**, *73*, 3430–3438. [[CrossRef](#)]
- Senkov, O.N.; Wilks, G.B.; Scott, J.M.; Miracle, D.B. Mechanical properties of Nb₂₅Mo₂₅Ta₂₅W₂₅ and V₂₀Nb₂₀Mo₂₀Ta₂₀W₂₀ refractory high entropy alloys. *Intermetallics* **2011**, *19*, 698–706. [[CrossRef](#)]
- Wen, J.; Chu, X.; Cao, Y.; Li, N. Effects of Al on Precipitation Behavior of Ti-Nb-Ta-Zr Refractory High Entropy Alloys. *Metals* **2021**, *11*, 514. [[CrossRef](#)]
- Chen, G.; Xiao, Y.; Ji, X.; Liang, X.; Hu, Y.; Cai, Z.; Liu, J.; Tong, Y. Effects of Zr Content on the Microstructure and Performance of TiMoNbZrx High-Entropy Alloys. *Metals* **2021**, *11*, 1315. [[CrossRef](#)]

7. Vellios, N.; Keating, P.; Tsakiroopoulos, P. On the Microstructure and Properties of the Nb-23Ti-5Si-5Al-5Hf-5V-2Cr-2Sn (at.%) Silicide-Based Alloy—RM(Nb)IC. *Metals* **2021**, *11*, 1868. [[CrossRef](#)]
8. Han, Z.D.; Luan, H.W.; Liu, X.; Chen, N.; Li, X.Y.; Shao, Y.; Yao, K.F. Microstructures and mechanical properties of TixNbMoTaW refractory high-entropy alloys. *Mater. Sci. Eng. A* **2018**, *712*, 380–385. [[CrossRef](#)]
9. Luo, G.; Jiang, S.; Kang, K.; Wang, X.; Zhang, J.; Sun, Y.; Shen, Q. Eutectic-like composite of MoNbWTaC with outstanding strength and plasticity at elevated temperature. *Mater. Lett.* **2021**, *304*, 130739. [[CrossRef](#)]
10. Xiao, B.; Jia, W.; Tang, H.; Wang, J.; Zhou, L. Microstructure and mechanical properties of WMoTaNbTi refractory high-entropy alloys fabricated by selective electron beam melting. *J. Mater. Sci. Technol.* **2022**, *108*, 54–63. [[CrossRef](#)]
11. Fu, T.; Cui, K.; Zhang, Y.; Wang, J.; Shen, F.; Yu, L.; Qie, J.; Zhang, X. Oxidation protection of tungsten alloys for nuclear fusion applications: A comprehensive review. *J. Alloys Compd.* **2021**, *884*, 161057. [[CrossRef](#)]
12. Schellert, S.; Gorr, B.; Laube, S.; Kauffmann, A.; Heilmaier, M.; Christ, H.J. Oxidation mechanism of refractory high entropy alloys Ta-Mo-Cr-Ti-Al with varying Ta content. *Corros. Sci.* **2021**, *192*, 109861. [[CrossRef](#)]
13. Wegener, T.; Klein, F.; Litnovsky, A.; Rasinski, M.; Brinkmann, J.; Koch, F.; Linsmeier, C. Energy Development of yttrium-containing self-passivating tungsten alloys for future fusion power plants. *Nucl. Mater.* **2016**, *9*, 394–398.
14. Flamini, C.; Ciccio, A.; Traverso, P.; Gnecco, F.; Giardini Guidoni, A.; Mele, A. Laser-induced evaporation, reactivity and deposition of ZrO₂, CeO₂, V₂O₅ and mixed Ce-V oxides. *Appl. Surf. Sci.* **2000**, *168*, 104–107. [[CrossRef](#)]
15. Ostovari Moghaddam, A.; Sudarikov, M.; Shaburova, N.; Zhrebtsov, D.; Zhivulin, V.; Ashurali Solizoda, I.; Starikov, A.; Veselkov, S.; Samoilo, O.; Trofimov, E. High temperature oxidation resistance of W-containing high entropy alloys. *J. Alloys Compd.* **2021**, 162733. [[CrossRef](#)]
16. Veselkov, S.; Samoilo, O.; Shaburova, N.; Trofimov, E. High-Temperature Oxidation of High-Entropic Alloys: A Review. *Materials* **2021**, *14*, 2595. [[CrossRef](#)] [[PubMed](#)]
17. Ostovari Moghaddam, A.; Shaburova, N.A.; Sudarikov, M.V.; Veselkov, S.N.; Samoilo, O.V.; Trofimov, E.A. High temperature oxidation resistance of Al_{0.25}CoCrFeNiMn and Al_{0.45}CoCrFeNiSi_{0.45} high entropy alloys. *Vacuum* **2021**, *192*, 110412. [[CrossRef](#)]
18. Li, L.-C.; Li, M.-X.; Liu, M.; Sun, B.-Y.; Wang, C.; Huo, J.-T.; Wang, W.-H.; Liu, Y.-H. Enhanced oxidation resistance of MoTaTiCrAl high entropy alloys by removal of Al. *Sci. China Mater.* **2021**, *64*, 223–231. [[CrossRef](#)]
19. Lo, K.-C.; Chang, Y.-J.; Murakami, H.; Yeh, J.-W.; Yeh, A.-C. An oxidation resistant refractory high entropy alloy protected by CrTaO₄-based oxide. *Sci. Rep.* **2019**, *9*, 7266. [[CrossRef](#)]
20. Gorr, B.; Müller, F.; Schellert, S.; Christ, H.-J.; Chen, H.; Kauffmann, A.; Heilmaier, M. A new strategy to intrinsically protect refractory metal based alloys at ultra high temperatures. *Corros. Sci.* **2020**, *166*, 108475. [[CrossRef](#)]
21. Tan, X.Y.; Klein, F.; Litnovsky, A.; Wegener, T.; Schmitz, J.; Linsmeier, C.; Coenen, J.W.; Breuer, U.; Rasinski, M.; Li, P.; et al. Evaluation of the high temperature oxidation of W-Cr-Zr self-passivating alloys. *Corros. Sci.* **2019**, *147*, 201–211. [[CrossRef](#)]
22. Morin, F.; Beranger, G.; Lacombe, P. Limits of application for Wagner's oxidation theory. *Oxid. Met.* **1972**, *4*, 51–62. [[CrossRef](#)]
23. Müller, F.; Gorr, B.; Christ, H.-J.; Müller, J.; Butz, B.; Chen, H.; Kauffmann, A.; Heilmaier, M. On the oxidation mechanism of refractory high entropy alloys. *Corros. Sci.* **2019**, *159*, 108161. [[CrossRef](#)]
24. Yamaguchi, O.; Mukaida, Y.; Shigeta, H. Preparation of Alkoxy-Derived Tantalum Vanadate. *J. Am. Ceram. Soc.* **1989**, *72*, 1914–1917. [[CrossRef](#)]
25. Pilling, N.; Bedworth, R.E. The oxidation of metals at high temperatures. *J. Inst. Met.* **1923**, *29*, 529.
26. Xu, C.; Gao, W. Pilling-Bedworth ratio for oxidation of alloys. *Mater. Res. Innov.* **2000**, *3*, 231–235. [[CrossRef](#)]